



UNIVERSITY OF LEEDS

This is an author produced version of *A characterization of cold pools in the West African Sahel*.

White Rose Research Online URL for this paper:
<http://eprints.whiterose.ac.uk/88489/>

Article:

Provod, M, Marsham, JH, Parker, D and Birch, C (2015) A characterization of cold pools in the West African Sahel. *Monthly Weather Review*. ISSN 1520-0493 (In Press)



*promoting access to
White Rose research papers*

eprints@whiterose.ac.uk
<http://eprints.whiterose.ac.uk/>

1
2
3
4
5
6
7
8
9
10
11
12
13
14
15
16
17
18
19
20
21
22
23
24
25
26
27
28
29
30
31
32
33
34
35
36
37
38
39
40
41
42
43
44

A characterization of cold pools in the West African Sahel

Authors and their institutions:

¹M Provod (University of Leeds), Email: eempr@leeds.ac.uk

Dr J H Marsham (Water @ Leeds, University of Leeds), Email: j.marsham@leeds.ac.uk

Prof D J Parker (University of Leeds), Email: d.j.parker@leeds.ac.uk

Dr Cathryn E Birch (Met Office @ Leeds), Email: cathryn.birch@metoffice.gov.uk

Institutional addresses:

School of Earth and Environment
The University of Leeds
Leeds, LS2 9JT
United Kingdom

¹ Corresponding author

45
46
47
48
49
50
51
52
53
54
55
56
57
58
59
60
61
62
63
64
65
66
67
68
69
70
71
72
73
74
75
76
77
78
79
80
81

Abstract

Cold pools are integral components of squall-line mesoscale convective systems and the West African Monsoon, but are poorly represented in operational global models. Observations of thirty-eight cold pools made at Niamey during the 2006 AMMA (African Monsoon Multidisciplinary Analysis) campaign (1 June to 30 September 2006), are used to generate a seasonal characterization of cold-pool properties by quantifying related changes in surface meteorological variables. Cold pools were associated with temperature decreases of 2 to 14°C, pressure increases of 0 to 8 hPa and wind gusts of 3 to 22 m s⁻¹. Comparison with published values of similar variables from the Great Plains of the USA showed comparable differences. The leading part of most cold pools had decreased water vapour mixing ratios compared to the environment, with moister air, likely related to precipitation, approximately 30 minutes behind the gust front. A novel diagnostic used to quantify how consistent observed cold pool temperatures are with saturated or unsaturated descent from mid-levels (Fractional Evaporational Energy Deficit, FEED) shows that early-season cold pools are consistent with less saturated descents. Early season cold pools were relatively colder, windier and wetter, consistent with drier mid-levels, although this was only statistically significant for the change in moisture. Late season cold pools tended to decrease equivalent potential temperature from the pre-cold-pool value, whereas earlier in the season changes were smaller, with more increases. The role of cold pools may therefore change through the season, with early season cold-pools more able to feed subsequent convection.

82
83
84
85
86
87
88
89
90
91
92
93
94
95
96
97 **1. Introduction**

98

99 Mesoscale convective systems (MCSs) form an integral part of the West African
100 Monsoon (Flamant *et al.* 2007; Marsham *et al.* 2013a) and account for more than 80% of
101 the annual rainfall in most of the Sahel (Mathon *et al.* 2002; Dhonneur, 1973). Cold pools
102 produced by MCSs are important for a number of reasons; they are a key mechanism for
103 maintenance of the MCSs, and for secondary initiation of new cumulonimbus systems; they
104 transport substantial amounts of cold air northwards, cooling and moistening the Saharan
105 heat-low by advection (Marsham *et al.* 2013; Garcia-Carreras *et al.* 2013), they are
106 responsible for around 50% of summertime dust uplift in the Sahel & Sahara (Marsham *et*
107 *al.* 2008; Marsham *et al.* 2011b; Heinold *et al.* 2013; Marsham *et al.* 2013b) and are
108 associated with intense rain and strong winds.

109

110 In the summer, seasonally increasing south-westerly monsoon winds advect moist
111 high equivalent potential temperature (Θ_e) low level air into the Sahel, which undercuts the
112 dry mid-level Saharan Air Layer (SAL; Parker *et al.* 2005a). The SAL is characterised by almost

113 dry adiabatic lapse rates, which together with the low-level moisture results in large
114 quantities of Convective Available Potential Energy (CAPE). There is, however, high
115 Convective Inhibition (CIN), which together with mid-tropospheric dry air needs to be
116 overcome for deep convection to be initiated and sustained.

117

118 Localised triggering initially creates discrete small-scale convective storms (Dione *et*
119 *al.*, 2013) that can, under certain conditions, grow upscale to form an MCS, often in the
120 form of a propagating squall line (Hamilton *et al.* 1945; Aspliden *et al.* 1976; Fortune, 1980;
121 Chong *et al.* 1987; Lebel *et al.*, 1997a, b; Futyan and Del Genio, 2007; Chong *et al.* 2010;
122 Lafore *et al.* 2010; Lothon *et al.* 2011; Birch *et al.* 2013). Due to the presence of mid-
123 tropospheric dry air masses in the Sahel, latent cooling caused by evaporation, melting or
124 sublimation of hydrometeors is supportive of the formation of a cooler than environment
125 downdraft (Redelsperger and Lafore, 1988). This cooler air then reaches the surface and
126 spreads out as a density current – the cold pool (Charba, 1974; Mueller and Carbone, 1987).
127 Together with the ambient wind shear, the cold pool helps to lift surrounding air parcels
128 (e.g. Dione *et al.*, 2013) and create new cells, organizing the MCS (Roca *et al.* 2005).
129 Therefore, cold pools play an important role in organizing deep moist convection and are an
130 integral part of MCSs (Thorpe *et al.* 1982; Rotunno *et al.* 1988; Weisman *et al.* 1988; Fovell
131 and Ogura 1989; Szeto and Cho 1994a, b; Trier *et al.* 1997; Parker and Johnson 2004a, b).

132

133 Perhaps the largest observational study of cold pool properties to date is based in
134 the USA over Oklahoma and was performed by Engerer *et al.* (2008; hereafter E2008). Their
135 study investigated 39 squall line MCSs by using data from 110 mesonet stations across the
136 state of Oklahoma and obtained 1389 time series of cold pool related variables. The cold

137 pool quantities studied by E2008 were decreases in potential and equivalent potential
138 temperature, pressure rises, changes in wind direction and maximum wind gusts. The focus
139 of their study was on the evolution of cold pool properties during various life cycles of MCSs
140 as well as comparison of the observed cold pool characteristics with idealised model
141 simulations. Given that this study was based in the USA, it is of interest to assess whether
142 the particular conditions of MCSs in West Africa result in comparable distributions of cold
143 pool properties. As far as the authors are aware, there are several case studies of West-
144 African MCSs (e.g. Chong *et al.* 2010; McGraw-Herdeg, 2010), but to date there is no general
145 characterization of surface cold-pool properties.

146

147 This paper studies observed properties of West African cold pools produced by
148 organized MCSs, mostly squall-lines, and compares them to results obtained in Oklahoma by
149 E2008. One goal of this paper is to provide observational results for future studies to better
150 evaluate cold pools in models. The monsoon season is split into three sub-periods to enable
151 evaluation of seasonal evolution of MCS-related cold pool properties. Section 2 describes
152 the observational data sets and the analysis method. Section 3*a* focuses on thermodynamic
153 properties such as pressure and temperature and their seasonal variations. Section 3*b*
154 studies cold-pool winds. Section 4 summarizes the results and discusses their implications.

155

156

157

158 **2. Data and methods**

159

160

161 **a. Data**

162

163 The African Monsoon Multidisciplinary Analysis Special Observing Period (AMMA
164 SOP) took place in 2006. Documentation of MCSs was one of the key components of AMMA
165 and the data obtained during AMMA currently provide the most detailed and complete
166 dataset for moist convection in West Africa (Redelsperger *et al.* 2006, Lebel *et al.* 2010).

167

168 The MIT (Massachusetts Institute of Technology) C-Band Doppler radar was
169 deployed near Niamey, Niger (13.5° N, 2.2°E) during AMMA. Scans were recorded at 10-
170 minute intervals during the AMMA Radar Observing Period (AMMA ROP), which ran from 5
171 July 2006 until 27 September 2006. For the purpose of this study we used 360° long-range
172 (250 km) surveys at 0.7° elevation in addition to Meteosat infrared satellite images.

173

174 The ARM (Atmospheric Radiation Measurement) Climate Research mobile facility
175 was deployed at Niamey airport. Surface meteorology data obtained from this station were
176 used in this study. The surface data consist of pressure, temperature, relative humidity, 10-
177 m winds and rainfall intensity. For the purpose of this study, these data were used to
178 calculate surface equivalent potential temperature and Water Vapour Mixing Ratio
179 (WVMR). These were available in minute-averaged intervals for the whole AMMA SOP.

180

181 Radiosondes were released daily from Niamey airport approximately 30 minutes
182 before 00, 06, 12 and 18 UTC. Some days had additional radiosonde releases approximately
183 30 minutes before 03, 09, 15 and 21 UTC. Local time is identical to UTC time (with solar
184 noon at 11:57 UTC on 15 July 2006). There were, however, days when radiosonde ascents

185 were missing or delayed.

186

187

188 **b. Method**

189

190 The study period spanned from 1st June to 30th September 2006. A very similar
191 approach to E2008 has been applied to allow comparison between West African MCS cold
192 pools and E2008's results from the USA. E2008 subjectively identified cold-pool crossing
193 times and then objectively quantified changes in surface station variables from the 30
194 minutes preceding the cold pool crossing to the two hours subsequent to the crossing. The
195 30 minute time window used to detect pre-storm maxima and minima in surface variables
196 used by E2008 was not always long enough to capture these in Niamey, mainly in case of
197 pressure as the pre-storm minimum was on average 52 minutes ahead of the cold pool.
198 Therefore, in this study, the pre-storm time window was extended to 1 hour before the cold
199 pool arrival time.

200

201 Time series of surface station data for an example cold pool, observed on 11th
202 August 2006 at Niamey Airport, are shown in Figure 1. Cold pool crossings are associated
203 with a sudden change in wind direction (Engerer *et al.* 2008; Fujita, 1963) and as in E2008
204 the wind direction change was considered as the main factor in the identification of crossing
205 times (e.g. Figure 1). Times of sudden wind direction changes were subjectively identified
206 and counted as potential cold pools. In order for the wind direction change to be sudden, it
207 must have happened within 5 minutes and been of at least 30-degree magnitude. Because a
208 wind direction change may, however, be associated with features other than cold pools (e.g.

209 dust devils (Tratt *et al.*, 2003), or gravity waves (Cram *et al.*, 1992, Birch *et al.*, 2013)), the
210 other surface variables were also considered as specified below.

211

212 The change in wind direction must have occurred within 30 minutes of a wind gust
213 and changes in temperature and pressure to be counted as cold-pool related. The
214 magnitude of the gust must have been at least 1.5 times greater than the mean wind speed
215 in the 30 minutes before the gust and temperature must have dropped by at least 1°C (e.g.
216 Figure 1). It is not likely, but possible, that something other than an MCS cold pool in the Sahel
217 would cause these changes in pressure, temperature and wind. Because of this limitation of
218 using surface data only, all the identified cold pools were verified by considering images
219 from the MIT radar or satellite (outside of the ROP). This verification has been done
220 subjectively based on inspection of radar/satellite images to see whether an MCS has been
221 present in the vicinity of Niamey at the time of the cold pool passage.

222

223 Following the approach of E2008, the cold pool related changes in surface variables
224 were calculated for: (1) increase in pressure (the maximum after the cold-pool minus the
225 minimum before), and (2) decrease in temperature (maximum before minus the minimum
226 after). For (3) equivalent potential temperature (Θ_e), cold pools could give an increase or a
227 decrease, and often short-lived fluctuations complicated any method based on minima and
228 maxima; therefore, unlike E2008, changes in mean from the period spanning 1 hour before
229 the cold-pool crossing-time to the period spanning 2 hours after the crossing were
230 calculated. In addition, unlike E2008, (4) change in water vapour mixing ratio (WVMR) and
231 (5) increase in mean wind speed were also calculated. For WVMR, the mean value in the
232 hour before the cold pool was subtracted from the minimum value in the 2 hours after (so

233 positive values show moistening). The minimum after the passage was used rather than
234 maximum as there was often a sharp minimum just following a cold pool passage, that was
235 often followed by an increase that reached greater than pre-cold pool magnitudes within
236 the 2 hours, but which was likely not primarily related to the cold pool crossing (e.g. Figure
237 1). The mean value in the 1 hour before the cold pool was used rather than a maximum in
238 order to take into account the sometimes sharp fluctuations in WVMR that were likely
239 related to turbulence and mixing. In addition, maximum wind gust associated with the cold
240 pool was obtained by taking maximum wind speed in the 2 hours after the cold pool
241 crossing (as in E2008).

242

243 For a majority of the studied cold pools, the cold-pool-related changes in surface
244 variables were coincident or nearly coincident. There were, however, several cases where
245 this was not the case and hence it was difficult to define the cold pool crossing time. This
246 was most frequent in case of wind-direction changes, where in several cases there were
247 multiple wind-direction changes of more than 30° within ~2 hours of a wind gust, but none
248 coincided with the actual wind gust. These were likely related to waves propagating faster
249 than the cold pool from the parent storm. In such cases either the time of the closest wind
250 direction change to the gust or the time of the actual gust was taken as the crossing time,
251 based on whichever was closest to the temperature drop. Because of this there is clearly
252 uncertainty in the cold pool crossing times, but E2008 show the objectively determined
253 changes are generally robust to the precise crossing time used.

254

255 Using the radar and Meteosat imagery, the storms generating the cold pools were
256 separated subjectively into isolated storms and larger organized convective systems (MCSs;

257 spanning at least 100km as defined by American Meteorological Society, 2014). The main
258 difference between the methods of E2008 and this study is that MCS lifecycle stage
259 differentiation was not used because there was one radar available in the Sahel, which is
260 not enough information to decide on the lifecycle stage as it covers only a fraction of the
261 MCSs lifecycle. Instead, data were separated by sub-periods.

262

263 It was hypothesised that cold pool intensity would depend on mid-level dryness.
264 Therefore, the whole season was divided into three sub-periods based on the seasonal
265 evolution of rainfall at Niamey (Figure 2). We refer to these sub-periods as: “Pre-monsoon”
266 (1st June 2006 – 12th July 2006), “Monsoon” (13th July 2006 – 27th August 2006) and
267 “Retreat” (27th August 2006 – 30th September 2006), although they are not based on any
268 formal definition of monsoon onset. The sub-period boundaries were set based on
269 subjectively-identified changes of slope in the observed time-series of accumulated rainfall
270 (clearest for pre-monsoon to monsoon). Out of the 38 cold pools used in this study, 22
271 occurred in the ‘monsoon’ sub-period with 8 in the ‘pre-monsoon’ and 8 in the ‘retreat’ sub-
272 periods.

273

274

275 **3. Results and discussion**

276

277 During the study period, 42 cold pools were detected. Of these, 33 were squall-line
278 MCSs (having a continuous line being at least 100 km in length and having reflectivity of at
279 least 35 dBz along at least 50% of its length), 4 were non-squall-line MCSs, one was a
280 propagating cold pool from a freshly dissipated MCS (seen in satellite imagery but out of

281 radar range) and 4 were from local non-MCS convection (there were many isolated
282 convective storms in the range of the MIT radar, but their cold pools rarely crossed Niamey).
283 The 4 cold pools related to the isolated convection gave very limited statistics and since this
284 study focuses on cold pools produced by organised MCS's, data from these 4 cases were not
285 used in the analysis.

286

287 Figure 3 shows composites of surface variables, centred on cold pool crossing time.
288 The “composite cold pool”, (over the entire observation period, black lines), was
289 accompanied by a decrease in temperature of 5.3°C. As expected, the cooling of the cold
290 pool brings a pressure increase, the magnitude of which was 1.9 hPa. The wind maximum
291 related to the cold pool passage had a magnitude of 6.5 m s⁻¹ in the composite, with the
292 wind rotating from approximately 200 to 120 degrees. Rainfall intensity increased rapidly to
293 a maximum about 15 minutes after the cold pool passage with a second peak approximately
294 45 minutes after the passage. The weaker precipitation behind the first peak corresponds to
295 the “weak echo” in the radar observations, between stratiform rain and the main line of
296 convective cells. WVMR decreased after the initial passage and stayed low throughout the
297 first “convective rainfall” maximum. Approximately 30 minutes after the cold pool passage,
298 there was a small increase of WVMR (accompanied by an increase in relative humidity, not
299 shown). Although only around 0.5 g kg⁻¹ this change is approximately twice the standard
300 error in the composite of cold-pool changes (not shown) and this temporary decrease
301 followed by an increase was observed in 26 out of 38 cases. The increase was coincident
302 with the second “stratiform” rainfall peak. This drying and moistening coincidence with the
303 rainfall suggests that there may be a descent of dry mid-level air towards the surface
304 occurring during the convective rainfall occurrence, while later evaporation of stratiform

305 rain increases WVMR.

306

307 Figure 3 shows that cold-pool related changes are different across the sub-periods.
308 Pre-monsoon cold pools are associated with greater pressure increases, temperature
309 decreases, less intense and shorter-lived precipitation and stronger winds. Furthermore, the
310 related changes in equivalent potential temperature and WVMR vary. The statistical
311 significance of these seasonal differences is investigated in later sections. All values given
312 below are means and standard deviations. The composite pre-monsoon cold pools caused a
313 long-lived WVMR increase of $2.5 \text{ g kg}^{-1} \pm 0.8 \text{ g kg}^{-1}$, while during the monsoon and retreat
314 there are long-lived decreases of 1.5 ± 0.2 and $2.7 \pm 0.5 \text{ g kg}^{-1}$ respectively. Equivalent
315 potential temperature changes very little with a pre-monsoon cold pool passage. In
316 contrast, there is a sharp and long-lived decrease in equivalent potential temperature in the
317 monsoon and retreat sub-periods, with the decrease during the retreat being greater than
318 during the monsoon ($11.9 \pm 10^\circ\text{C}$ and $7.8 \pm 4^\circ\text{C}$ respectively). The rainfall structure of pre-
319 monsoon MCSs also appears to be different: the two rainfall peaks are less clear and later
320 stratiform rain makes a smaller contribution to the total.

321

322 **a) Thermodynamic properties of cold pools**

323

324 Figure 4 shows bar plots of the normalised frequency distribution of several cold
325 pool properties and their seasonal variations. The bars are normalized to allow comparison
326 between sub-seasons and account for the different numbers of cold pools identified in the
327 three sub-periods. There were 8 events each in “pre-monsoon” and “retreat” and 22 in
328 “monsoon”; therefore “monsoon” was normalised by multiplying the number of events by

329 8/22 to allow comparison. The black line which shows the frequency distribution over all
330 three sub-periods therefore only overlies the top of the bar plots when there are no
331 “monsoon” events in that bin. .

332

333 A temperature decrease between 1.8 °C and 13.1 °C was observed for all cold pool
334 passages (Figure 4a). The whole seasonal distribution is skewed however, with a broad peak
335 between approximately 3 °C and 7 °C and only 3 events of temperature decrease greater
336 than 11 °C. The distribution of pressure increase in Figure 4b is also skewed, ranging from
337 0.4 to 7.6 hPa, with most events between 1 and 4 hPa. These values are larger than the
338 pressure increase in the cold pool composite in Figure 3 because the timing of the maximum
339 and minimum pressure relative to the gust-front differs between cold pools. This is a
340 limitation of the composite as minima and maxima occur at relatively different times from
341 the time of crossing; partly because cold pools propagate at different speeds and also
342 because for any system the maxima/minima are located at different positions relative to the
343 gust front.

344

345 Figure 4c shows that the majority of cold pools led to a drying, but 10 cold pools
346 (27%) led to an increase in WVMR. The WVMR increase ranged from -3.4 g kg⁻¹ to +6.1 gkg⁻¹.
347 Most events gave a decrease in mean Θ_e with the greatest decrease being -12.6 °C but
348 several events show an increase, with the largest being +8.7 °C (Figure 4d). Bar plots of
349 relative humidity are not shown, but it was found that all cold pools gave increases in RH of
350 magnitudes between 0 and 60%. It was found that the three cold pools with greatest WVMR
351 increases were closest to rain, but no overall relationship could be concluded between the
352 WVMR change and its proximity to rainfall.

353

354 There was a tendency towards greater pressure increases and temperature
355 decreases in the pre-monsoon period when compared to the whole season (mean changes
356 were 3.4 hPa for pre-monsoon compared to 2.9 hPa overall and 7.8 °C compared with
357 5.9 °C overall). The differences in pressure and temperature changes between sub-seasons
358 were, however, not statistically significant at the 90% level. Humidity changes from cold
359 pools also varied across the sub-periods, with WVMR tending to increase in pre-monsoon,
360 but tending to decrease in the rest of the season (means of +1.1 g kg⁻¹ for pre-monsoon
361 compared with -0.6 gkg⁻¹ overall). Mean equivalent potential temperature both increased
362 and decreased in the pre-monsoon, but nearly always decreased in the remainder of the
363 observation period (mean changes of -2.2°C compared with -9.6 °C). The seasonal
364 differences in changes equivalent potential temperature and WVMR were significant at the
365 90% level. This pre-monsoon difference is consistent with drier mid-levels during the pre-
366 monsoon period that promote more evaporation (or sublimation) and hence greater
367 associated moistening, cooling and greater pressure increases, although the differences
368 were only statistically significant for the moistening (see also section 3a 1). It is also
369 consistent with Garcia-Carreras, *et al.* (2013) who shows that cold pools carry moisture
370 northwards into the Sahara from the Sahel during the pre-monsoon period.

371

372 Figures 5a and 5b show that colder cold pools give larger pressure increases, as
373 expected. This relationship is most consistent for pre-monsoon cases, which have a
374 correlation of 0.6 (statistically significant at $p < 0.11$), with monsoon and retreat periods
375 having only weak correlations of 0.08 and -0.2 respectively (not statistically significant). The
376 overall correlation for the season was 0.3 (statistically significant at $p < 0.07$).

377

378 The overall distribution in Figure 5a is similar to that shown in Figure 5 of E2008,
379 except that a small percentage of cold pools in Engerer's study (1.5%) had either larger
380 pressure increases or temperature deficits. Based on the total number of data points and
381 the data points with temperature decrease greater than 14 °C or pressure increase greater
382 than 7 hPa in E2008, we would expect approximately 0.6 data-points with magnitudes of at
383 least 14 °C or 7 hPa for temperature decrease and pressure increase respectively to be
384 found in our study if magnitudes of cold pool properties in Niamey were identical to those in
385 Oklahoma. The fact that there were no such cold pools in our study, however, is not
386 statistically significant at the 0.05 significance level to conclude that cold pools in Niamey
387 are weaker in terms of temperature decrease and pressure increase when compared to
388 Oklahoma. A considerably larger data-set would be needed to make any conclusions about
389 the occurrence of such strong cold pools in Niamey when compared to Oklahoma. Note that
390 MCSs tend to be observed at a particular point in their lifecycle in Niamey. This was often
391 either in a mature or dissipating stage, although difficult to differentiate at times due to only
392 one radar data source and attenuation by rainfall as already discussed. Hence, stronger cold
393 pools may be observed elsewhere in West Africa. This is a limitation of this observational
394 study, which was, by necessity, confined to one spatial point.

395

396 Observed night-time cold pools are generally associated with higher values of
397 pressure increase for a given temperature decrease than day-time ones (Figure 5b). The
398 reason for this is likely the fact that at night the boundary layer tends to be stable due to
399 nocturnal cooling and during the day the surface layer is unstable. The magnitude of the
400 cold pool related change in temperature aloft is therefore greater than observed at the

401 surface at night, and less during the day (Davies *et al.* 2005). The cold pool may also slide on
402 top of the stably stratified surface layer at night (Heinold *et al.* 2013; Marsham 2011a),
403 significantly reducing the temperature decrease measured at the surface. However, both
404 small and large decreases in surface temperature in Figure 5b show that at least some of
405 downdrafts at Niamey routinely reach the surface despite the presence of a nocturnal inversion.
406 Figure 5b shows that pressure increases greater than ~ 5 hPa occurred only at night or in the
407 morning (before 8am), which is consistent with E2008 and likely the result of deeper cold
408 pools associated with maturing/dissipating MCSs and the known tendency for large
409 organised systems at night over Niamey (Rickenbach *et al.* 2009).

410

411 **1) Role of mid-level dryness**

412 It was hypothesised that the stronger cold pools in the pre-monsoon period (with
413 greater wind gusts, see section 3b) may be caused by seasonally drier mid-levels in that
414 period (Marsham *et al.* 2008; Barnes and Sieckman 1984). We test this hypothesis using a
415 one-dimensional conceptual model, where radiosonde data were used to quantify mid-level
416 dryness for each cold pool using Θ_w (wet-bulb potential temperature) depression (i.e.
417 difference between Θ and Θ_w averaged between 550 and 750 hPa) using the nearest pre-
418 storm sounding. These soundings were between 38 minutes and 5 hours 52 minutes before
419 the cold pool crossing. Despite the long gaps between the radio-sounding and the cold pool
420 in some cases, these were the best mid-level data available. In reality, the applicability of
421 the one-dimensional model may be limited by significant horizontal gradients and
422 transports; this may in future be tested in high-resolution modelling studies.

423

424 Figure 6 shows how close observed cold pool temperatures are to idealised descents

425 of mid-level air. In this figure, we plot “departure from moist adiabat” (DMA), defined as
426
$$\text{DMA} = \Theta_{\text{cold pool}} - \text{mean}(\Theta_w \text{ (550 to 750 hPa)})$$

427 Against mid-level dryness defined using the difference between mean potential
428 temperature and wet-bulb potential temperature in the 550 to 750 hPa layer. Therefore Fig.
429 6 shows how the cold pool potential temperature minus the wet-bulb potential
430 temperature of mid-levels (y-axis) depends on the mid-level Θ_w depression. If mid-level air
431 was cooled by evaporation of precipitation and descended whilst being kept saturated by
432 continued evaporation then the air would descend moist adiabatically and the cold pool
433 potential temperature would equal the mid-level Θ_w (y-axis value equals zero in Fig. 6). In
434 contrast, if mid-level air instead descended completely dry-adiabatically then the potential
435 temperature of the cold pool would equal the potential temperature of the mid-levels and
436 data would lie on the one-to-one line in Fig. 6. Therefore, how far the data are from the
437 one-to-one towards the x-axis line in Fig. 6 is a measure of the degree of saturation in the
438 idealised one-dimensional descent. We therefore refer to the y-axis as the “Departure from
439 Moist Adiabat” (DMA) and the ratio of both axes as the “Fractional Evaporational Energy
440 Deficit” (FEED), with the one-to-one line of FEED = 100%.

441

442 The values in Figure 6 can also be related to the energetics of the downdraught. For
443 a fixed pressure of source air, the potential energy of cooling by evaporation is
444 approximately proportional to the x-axis value (the energy is proportional to the tephigram-
445 area bounded by the Θ_w line of saturated descending air and the theta-line for unsaturated
446 descending air, and here we approximate this by a triangle). As noted above, if FEED is zero,
447 then the downdraught is fully saturated in its descent, and we could regard DCAPE
448 (Downdraft Convective Available Potential Energy) to be a good measure of the

449 downdraught potential energy released.

450

451 Figure 6 shows that $\Theta_{\text{cold pool}}$ values are never equal to mid-level Θ_w values, with the
452 moistest cold pool having DMA of 3.6 °C, confirming that no cold pool in our study was
453 formed by the theoretical, perfectly moist adiabatic descent of mid-level air. In contrast, the
454 highest value of DMA is 16.1 °C. All data points lie below the line of FEED of 67% and the
455 lowest data point has a FEED of 17.6%. The overall relationship suggests that drier mid-
456 levels are related to greater DMA and FEED (correlation between DMA and mid-level Θ_w
457 depression is 0.5 with $p < 0.001$, correlation between FEED and mid-level Θ_w depression is
458 0.03 with $p < 0.89$). This suggests that the ability of precipitation to keep the descending
459 parcel saturated decreases with drier mid-levels, which may be due to greater mixing of dry
460 air or insufficient availability of precipitation to be evaporated into the descending parcel.
461 Pre-monsoon data points have generally greater percentages of FEED and lie closer to the
462 FEED of 67% line. This is not statistically significant, but suggests that the drier atmosphere
463 in the pre-monsoon period may lead to drier descents.

464

465 **b) Cold-pool winds**

466

467 The observed maximum wind gusts range from 4 to 22 ms^{-1} with most cold pools
468 having gusts between 2.5 and 12.5 m s^{-1} (Figure 7a). The mean wind can either increase (26
469 cases) or decrease (11 cases) during a cold pool passage, with the magnitudes of increase
470 generally between 0 and 6 ms^{-1} , with the greatest value of increase being $\sim 10 \text{ms}^{-1}$ (Figure
471 7b). The magnitudes of the decreases were less than 3 ms^{-1} and were always associated with
472 a mean decrease of the general environmental wind speed.

473

474 The mean for maximum wind gusts in the pre-monsoon period was 10.1 ms^{-1} , which
475 was greater than that in the monsoon and retreat periods (7.6 and 7.5 ms^{-1} respectively).
476 This difference was, however, not statistically significant. There were comparable mean
477 wind-speed changes ($+1.4$, $+1.6$ and $+1.4$ for pre-monsoon, monsoon and retreat
478 respectively). The mean pre-monsoon gusts were strongly affected by a single strong event
479 on 17th June, when the highest gust of 21.4 ms^{-1} was recorded. If this case was removed
480 then the mean pre-monsoon gust decrease to 8.5 ms^{-1} (still higher than other sub-periods,
481 but again not significantly).

482

483 The relation between pressure changes and maximum wind gusts, which are partly
484 driven by the pressure changes, has a correlation of 0.46 ($p < 0.004$ – statistically significant)
485 (Figure 8). There was one outlier (the 17th June event), where additional features such as
486 mixing of momentum from upper levels may have caused stronger winds than would be
487 expected from the observed pressure increase alone. If this outlier is taken away, the
488 correlation reduces to 0.42 ($p < 0.01$, still statistically significant). The diurnal distribution of
489 cold pool related wind gusts shows that the higher cold-pool related gusts (above $\sim 10 \text{ ms}^{-1}$)
490 weren't limited to the daytime. This contradicts the fact that the stably stratified nocturnal
491 boundary layer can inhibit cold-pool winds at night (Parker 2008; Marsham *et al.* 2011a);
492 cold pools over Niamey from some of the mature nocturnal MCSs can clearly mix down
493 through this night-time stable layer (see also temperature changes in section 3a).

494

495

496 **4. Conclusions**

497

498 MCSs are an important feature of the West African Monsoon, providing most of the
499 rainfall over the Sahel. Cold pools contribute to the organisation of these MCSs, form a
500 crucial component of the monsoon flow (Marsham *et al.* 2013) and ventilate the Saharan
501 heat low (Garcia-Carreras *et al.* 2013). This study has quantified properties of cold pools
502 from MCSs observed over Niamey in the Sahel during the 2006 AMMA field campaign, using
503 a methodology similar to E2008.

504

505 Every observed cold pool in this study was associated with a temperature decrease,
506 ranging from 1.8 °C to 13.6 °C, and a pressure increase, ranging from 0.4 hPa to 8.1hPa.
507 These observed ranges generally agree with those observed by E2008 in the USA, but are
508 missing E2008's largest values. Given the much smaller sample size of our study, it is not
509 possible to say whether these more intense events are rarer in Niamey than the USA or
510 whether our sample is too small to observe them.

511

512 Water vapour mixing ratio was found to decrease just after the cold pool passage in
513 all but 9 cases. The magnitude of the decrease did not exceed 3.4 g kg⁻¹. This initial decrease
514 was in many cases followed by an increase in the mixing ratio of around 0.5 g kg⁻¹,
515 sometimes to values greater than before the cold pool passage, which appears to be
516 generated by the MCS rainfall. The mean equivalent potential temperature was found to
517 increase in 6 out of the 38 cases, but decrease in others. A maximum in observed winds has
518 been identified with every passage of an MCS, ranging from 3.7 ms⁻¹ to 21.6 ms⁻¹. The time-
519 averaged 10-m mean wind from before to after the gust front was found to usually increase,
520 although decreases were observed, with changes ranging from -2.3 to +10.0 ms⁻¹.

521

522 Cold pools in the pre-monsoon period gave larger pressure increases and temperature
523 decreases, as well as larger maximum wind gusts and mean wind increases, when compared
524 to the monsoon and retreat periods. These were, however, not statistically significant. Pre-
525 monsoon cold pools increased rather than decreased WVMR. Pre-monsoon cases gave little
526 overall change in equivalent potential temperature, which tended to be decreased by cold
527 pools in the monsoon and retreat periods. These differences in changes in WVMR and Θ_e
528 between cold pools during the pre-monsoon and later periods were statistically significant
529 at the 90% significance level. Furthermore, we define the Departure from Moist Adabat
530 (DMA) and Fractional Evaporational Energy Deficit (FEED) and use a simple 1D model to
531 quantify how close the observed cold pools were near wet adiabatic (FEED=0%) or dry
532 adiabatic (FEED=100%) descent. FEED varied from 17.6% to 64.5%, with drier descents for
533 drier mid-levels and during the pre-monsoon period (with only a correlation of 0.5 between
534 DMA and mid-level Θ_w depression). The importance of cold pools in the Sahel suggests that
535 future studies should use AMMA observations to evaluate modelled cold pools in
536 operational and research models. Such evaluations could make use of DMA and FEED as
537 defined here, which would be strengthened by trajectory analyses from a high-resolution
538 model.

539

540 The results show that early season cold pools provide high equivalent potential
541 temperature air at low levels, which especially if reheated could feed later convection, once
542 the high CIN is overcome (see also Torri *et al.*, 2015). Later in the season, the cold pools
543 reduce equivalent potential temperature but will still favor convection by lifting. The results
544 are consistent with observations from Garcia-Carreras *et al.* (2013), who show that cold

545 pools bring moist air towards the Saharan heat low early in the season. The results support
546 the hypothesis that early in the monsoon season, when mid-levels are drier and there is
547 therefore greater diabatic cooling, cold pools will make a greater contribution to the
548 monsoon flow (Marsham *et al.*, 2013).

549

550

551 **Acknowledgements**

552

553 We would like to thank all the reviewers for their constructive and helpful comments.
554 Surface meteorological data were obtained from the ARM Climate Research Facility (U.S.
555 Department of Energy) deployed in Niamey in the AMMA campaign. Based on a French
556 initiative, AMMA (<http://www.amma-international.org>) was built by an international group.
557 MIT radar was made available to AMMA from Massachusetts Institute of Technology.
558 AMMA-UK has been funded by NERC grants NE/B505538/1 and NE/G018499/1. Thanks to
559 Richard Pope and many others for practical help with using data analysis software.

560

561

562 **References**

563 Aspliden, C. I., 1976: Classification of Structure of Tropical Atmosphere and Related Energy
564 Fluxes. *J. App. Meteor.*, **15**, 692-697.

565 Barnes, G. M., and Sieckman, K., 1984: The Environment of Fast-Moving and Slow-
566 Moving Tropical Mesoscale Convective Cloud Lines. *Mon. Wea. Rev.*, **112**, 1782-1794.

567 Birch, C. E., D. J. Parker, A. O'Leary, C. M. Taylor, J. H. Marsham, P. Harris and G. Lister, 2013:

568 The impact of soil moisture and atmospheric waves on the development of a

569 mesoscale convective system: A model study of an observed AMMA case, *Q. J. R.*

570 *Meteor. Soc.*, **139**, 1712-1730.

571 Charba, J., 1974: Application of Gravity Current Model to Analysis of Squall-Line Gust Front.
572 *Mon. Wea. Rev.*, **102**, 140-156.

573 Chong, M., Amayenc, P., Scialom, G., and Testud, J., 1987: A Tropical Squall Line Observed
574 during the Copt-81 Experiment in West-Africa .1. Kinematic Structure Inferred from
575 Dual-Doppler Radar Data. *Mon. Wea. Rev.*, **115**, 670-694.

576 Chong, M., 2010: The 11 August 2006 squall-line system as observed from MIT Doppler
577 radar during the AMMA SOP. *Q. J. R. Meteor. Soc.*, **136**, 209-226.

578 Cram, J. M., Pielke, R. A., and Cotton and W. R., 1992: Numerical-Simulation and Analysis of
579 a Prefrontal Squall Line .2. Propagation of the Squall Line as an Internal Gravity-
580 Wave. *J. Atmos. Sci.*, **49**, 209-225.

581 Davies, T., Cullen, M. J. P., Malcolm, A. J., Mawson, M. H., Staniforth, A., White, A. A., &
582 Wood, N., 2005: A new dynamical core for the Met Office's global and regional
583 modelling of the atmosphere. *Q. J. R. Meteor. Soc.*, **131**(608), 1759-1782.

584 Dhonneur, G., 1973: Study of a Line Squall in Niger Bend. *Bull. Amer. Meteor. Soc.*, **54**, 1075-
585 1075.

586 Dione, C., M. Lothon, D. Badiane, B. Campistron, F. Couvreur, F. Guichard, and S. Salle,
587 2013: Phenomenology of Sahelian convection observed in Niamey during the
588 early monsoon. *Q. J. R. Meteor. Soc.*, **140**, 500-516.

589 Dixon, N. S., Parker, D. J., Taylor, C. M., Garcia-Carreras, L., Harris, P. P., Marsham, J. H., and
590 Woolley, A., 2013: The effect of background wind on mesoscale circulations above
591 variable soil moisture in the Sahel *Q. J. R. Meteor. Soc.*, **139**, 1009-1024.

592 Engerer, N. A., Stensrud, D. J., and Coniglio, M. C., 2008: Surface Characteristics of Observed
593 Cold Pools. *Mon. Wea. Rev.*, **136**, 4839-4849.

594 Flamant, C., Chaboureaud, J. P., Parker, D. J., Taylor, C. A., Cammas, J. P., Bock, O. Pelon, J.,
595 2007: Airborne observations of the impact of a convective system on the planetary
596 boundary layer thermodynamics and aerosol distribution in the inter-tropical
597 discontinuity region of the West African Monsoon. *Q. J. R. Meteor. Soc.*, **133**, 1175-
598 1189.

599 Fortune, M., 1980: Properties of African Squall Lines Inferred from Time-Lapse Satellite
600 Imagery. *Mon. Wea. Rev.*, **108**, 153-168.

601 Fovell, R. G., and Ogura, Y., 1989: Effect of Vertical Wind Shear on Numerically Simulated
602 Multicell Storm Structure. *J. Atmos. Sci.*, **46**, 3144-3176.

603 Fujita, T., 1963: Precise Reduction of Radiation Data from Meteorological Satellites. *J. Opt.*
604 *Soc. America*, **53**, 1331-&.

605 Futyan, J. M., and Del Genio, A. D., 2007: Deep convective system evolution over Africa and
606 the tropical Atlantic. *J. Climate*, **20**, 5041-5060.

607 Garcia-Carreras, L., Marsham, J. H., Parker, D. J., Bain, C. L., Milton, S., Sachi and A.
608 Washington, R., 2013: The impact of convective cold pool outflows on model biases
609 in the Sahara. *Geo. Res. Lett.*, **40**, 1647-1652.

610 Hamilton, R. A., and Archbold, J. W., 1945: Meteorology of Nigeria and Adjacent Territory. *Q.*
611 *J. R. Meteor. Soc.*, **71**, 231-&.

612 Heinold, B., Knippertz, P., Marsham, J. H., Fiedler, S., Dixon, N. S., Schepanski and K.Tegen, I.,
613 2013: The role of deep convection and nocturnal low-level jets for dust emission in
614 summertime West Africa: Estimates from convection-permitting simulations. *J. Geo.*
615 *Res. Atmos.*, **118**, 4385-4400.

616 Lafore, J. P., Redelsperger, J. L., and Jaubert, G., 1988: Comparison between a 3-Dimensional
617 Simulation and Doppler Radar Data of a Tropical Squall Line - Transports of Mass,
618 Momentum, Heat, and Moisture. *J. Atmos. Sci.*, **45**, 3483-3500.

619 Lebel, T., Taupin, J. D., and D'Amato, N., 1997a: Rainfall monitoring during HAPEX-Sahel .1.
620 General rainfall conditions and climatology. *J. Hyd.*, **189**, 74-96.

621 Lebel, T., and LeBarbe, L., 1997b: Rainfall monitoring during HAPEX-Sahel .2. Point and areal
622 estimation at the event and seasonal scales. *J. Hyd.*, **189**, 97-122.

623 Lothon, M., Campistron, B., Chong, M., Couvreux, F., Guichard, F., Rio, C., and Williams, E.,
624 2011: Life Cycle of a Mesoscale Circular Gust Front Observed by a C-Band Doppler
625 Radar in West Africa. *Mon. Wea. Rev.*, **139**, 1370-1388.

626 Marsham, J. H., Dixon, N. S., Garcia-Carreras, L., Lister, G. M. S., Parker, D. J., Knippertz, P.,
627 and Birch, C. E., 2013a: The role of moist convection in the West African monsoon
628 system: Insights from continental-scale convection-permitting simulations. *Geo. Res.*
629 *Let.*, **40**, 1843-1849.

630 Marsham, J. H., Hobby, M., Allen, C. J. T., Banks, J. R., Bart, M., Brooks, B. J., and
631 Washington, R., 2013b: Meteorology and dust in the central Sahara: Observations
632 from Fennec supersite-1 during the June 2011 Intensive Observation Period. *J. Geo.*
633 *Res. Atmos.*, **118**, 4069-4089.

634 Marsham, J. H., Trier, S. B., Weckwerth, T. M., and Wilson J. W., 2011a: Observations of
635 Elevated Convection Initiation Leading to a Surface-Based Squall Line during 13 June
636 IHOP_2002. *Mon. Wea. Rev.*, **139**, 247-271.

637 Marsham, J. H., Knippertz, P., Dixon, N. S., Parker, D. J., and Lister, G. M. S., 2011b: The
638 importance of the representation of deep convection for modelled dust-generating
639 winds over West Africa during summer. *Geo. Res. Let.*, **38**.

640 Marsham, J. H., Parker, D. J., Grams, C. M., Taylor, C. M., and Haywood, J. M., 2008: Uplift of
641 Saharan dust south of the intertropical discontinuity. *J. Geo. Res. Atmos.*, **113**

642 Mathon, V., Laurent, H., and Lebel, T., 2002: Mesoscale convective system rainfall in the
643 Sahel. *J. App. Meteor.*, **41**, 1081-1092.

644 McGraw-Herdeg, M., 2010: Dusty gust fronts and their contributions to long-lived
645 convection in West Africa. Ph.D. thesis, Department of Electrical Engineering and
646 Computer Science.

647 Mueller, C. K., and Carbone, R. E., 1987: Dynamics of a Thunderstorm Outflow. *J. Atmos. Sci.*,
648 **44**, 1879-1898.

649 Parker, M. D., and Johnson, R. H., 2004a: Simulated convective lines with leading
650 precipitation. Part I: Governing dynamics. *J. Atmos. Sci.*, **61**, 1637-1655.

651 Parker, M. D., and Johnson, R. H., 2004b: Simulated convective lines with leading
652 precipitation. Part II: Evolution and maintenance. *J. Atmos. Sci.*, **61**, 1656-1673.

653 Parker, DJ, Thorncroft CD, Burton RR, Diongue-Niang A., 2005a: Analysis of the African
654 easterly jet, using aircraft observations from the JET2000 experiment, Q.J.R. *Meteor.*
655 *Soc.*, **131**, 1461-1482.

656 Parker, M.D., 2008: Response of simulated squall lines to low-level cooling. *J. Atmos. Sci.*, **65**,
657 1323-1341.

658 Redelsperger, J. L., and Lafore, J. P., 1988: A 3-Dimensional Simulation of a Tropical Squall
659 Line - Convective Organization and Thermodynamic Vertical Transport. *J. Atmos. Sci.*,
660 **45**, 1334-1356.

661 Redelsperger, J. L., Thorncroft, C. D., Diedhiou, A., Lebel, T., Parker, D. J., and Polcher, J.,
662 2006: African monsoon multidisciplinary analysis - An international research project
663 and field campaign. *Bull. Amer. Meteor. Soc.*, **87**, 1739-+.

664 Rickenbach, T., Ferreira, R. N., Guy, N., and Williams, E., 2009: Radar-observed squall line
665 propagation and the diurnal cycle of convection in Niamey, Niger, during the 2006
666 African Monsoon and Multidisciplinary Analyses Intensive Observing Period. *J. Geo.*
667 *Res. Atmos.*, **114**.

668 Roca, R., Louvet, S., Picon, L., and Desbois, M., 2005: A study of convective systems, water
669 vapour and top of the atmosphere cloud radiative forcing over the Indian Ocean
670 using INSAT-1B and ERBE data. *Meteor. and Atmos. Phys.*, **90**, 49-65.

671 Rotunno, R., Klemp, J. B., and Weisman, M. L., 1988: A Theory for Strong, Long-Lived Squall
672 Lines. *J. Atmos. Sci.*, **45**, 463-485.

673 Szeto, K. K., and Cho, H. R., 1994a: A Numerical Investigation of Squall Lines .1. The Control
674 Experiment. *J. Atmos. Sci.*, **51**, 414-424

675 Szeto, K. K., and Cho, H. R., 1994b: A Numerical Investigation of Squall Lines .2. The
676 Mechanics of Evolution. *J. Atmos. Sci.*, **51**, 425-433.

677 Taylor, C. M., Harding, R. J., Thorpe, A. J., and Bessemoulin, P., 1997: A mesoscale simulation
678 of land surface heterogeneity from HAPEX-Sahel. *J. Hyd.*, **189**, 1040-1066.

679 Thorpe, A. J., Miller, M. J., and Moncrieff, M. W., 1982: Two-Dimensional Convection in Non-
680 Constant Shear - a Model of Mid-Latitude Squall Lines. *Q. J. R. Meteor. Soc.*, **108**, 739-
681 762.

682 Torri, G., Kuang Z., and Tian Y., 2015: Mechanisms for convection triggering by cold pools.
683 *Geo. Res. Lett.*

684 Tratt, D. M., Hecht, M. H., Catling, D. C., Samulon, E. C., and Smith, P. H., 2003: In situ
685 measurement of dust devil dynamics: Toward a strategy for Mars. *J. Geo. Res. Plan.*,
686 **108**.

687 Trier, S. B., Skamarock, W. C., and LeMone, M. A., 1997: Structure and evolution of the 22

688 February 1993 TOGA COARE squall line: Organization mechanisms inferred from
689 numerical simulation. *J. Atmos. Sci.*, **54**, 386-407.

690 Weisman, M. L. and J. B. Klemp *et al.*, 1988: Structure and Evolution of Numerically
691 Simulated Squall Lines. *J. Atmos. Sci.* **45**(14): 1990-2013.

692

693

694 **List of Figures**

695 **Figure 1:** *An example of an observed daily time series as obtained by the surface station at*
696 *Niamey airport. This time series is for 11th August 2006, when a cold pool crossing was*
697 *identified at 03:15 Local Time (denoted by vertical red line). Black lines denote the borders of*
698 *the time-windows used for the analysis. Solid lines correspond to left-hand axis and dashed*
699 *lines to right-hand axes. Data recorded every second and averaged at minute intervals.*

700 **Figure 2:** *Total accumulated rainfall from Niamey ARM surface station data. Red lines*
701 *separate three seasonal periods used in this study: "Pre-monsoon" (1st June 2006 – 12th July*
702 *2006); "Monsoon" (13th July 2006 – 27th August 2006); "Retreat" (27th August 2006 – 30st*
703 *September 2006).*

704 **Figure 3:** *Composite cold pools obtained from averaging variables of all cold pools around*
705 *the crossing time. Black line is for the whole period, red for the Pre-Monsoon period, blue for*
706 *the Monsoon and green for Retreat. The vertical pink line shows the cold pool crossing time.*

707 **Figure 4:** *Changes in specified thermodynamic variables from cold pools: a) Decrease in*
708 *temperature; b) Increase in pressure; c) Increase in WVMR; d) Increase in mean Θ_e .*

709 *Colouring represents the sub-periods (red: Pre-monsoon, blue: Monsoon, green: Retreat).*

710 *Number of events in each season is normalised to allow a comparison between seasons (see*
711 *text) with the black line showing total (unnormalised) distributions.*

712 **Figure 5** Pressure increases and temperature decreases from cold pools. Colouring in (a)
713 represents the whole period and sub-periods as in Figure 3. Colouring in (b) represents the
714 time of day (red: 8 – 16 UTC, blue: 18 – 6 UTC, green: 6-8 UTC, there were no events between
715 16 and 18 UTC).

716 **Figure 6:** Departure from Moist Adabat (DMA) which equals $(\Theta_{cold\ pool} - \text{mean}(\Theta_w(550\ to\ 750\ hPa)))$
717 versus mid-level dryness defined using the difference between mean $(\Theta(550\ to\ 750\ hPa))$
718 and mean $(\Theta_w(550\ to\ 750\ hPa))$. Colouring of points represents the sub-periods as in Figure 3.
719 Diagonal lines represent constant Fractional Evaporational Energy Deficit (FEED) of 100%
720 (black), 67% (blue) and 33% (red).

721 **Figure 7:** As Figure 4, but for (a) 10m wind gusts and (b) mean wind increases.

722 **Figure 8:** Cold pool pressure increases and maximum wind gusts. Colours represent different
723 times of day (red: 8-17 UTC, blue: 19-6 UTC, green: 6-8 UTC, no cold pool crossed between
724 17-19 UTC).

725

726

727

728

729

730

731

732

733

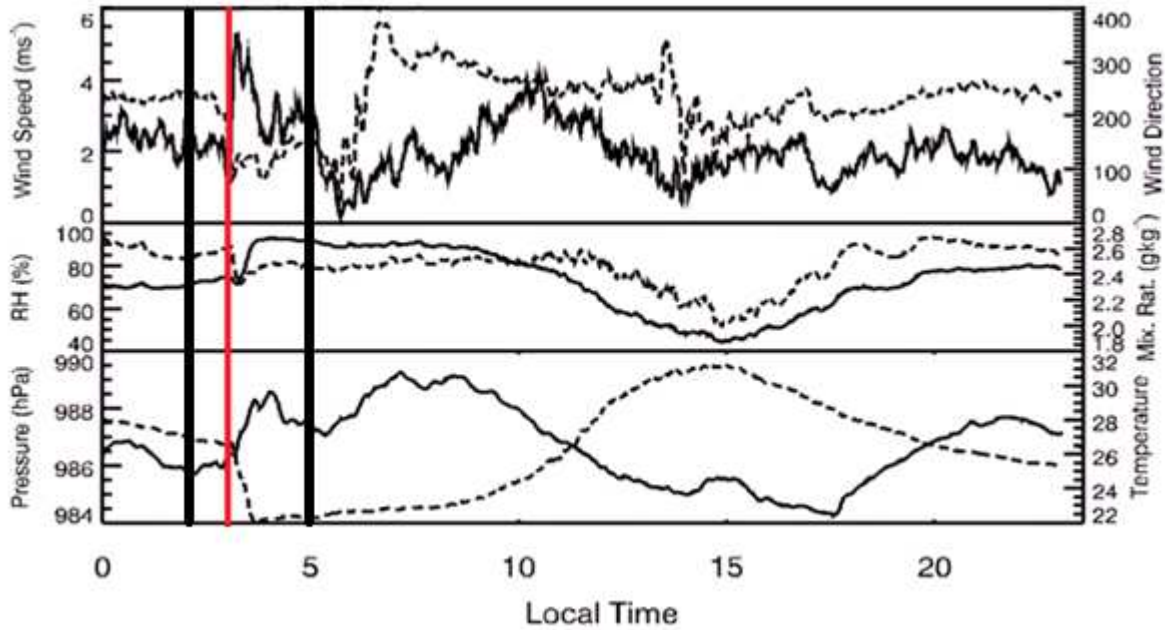
734

735

736

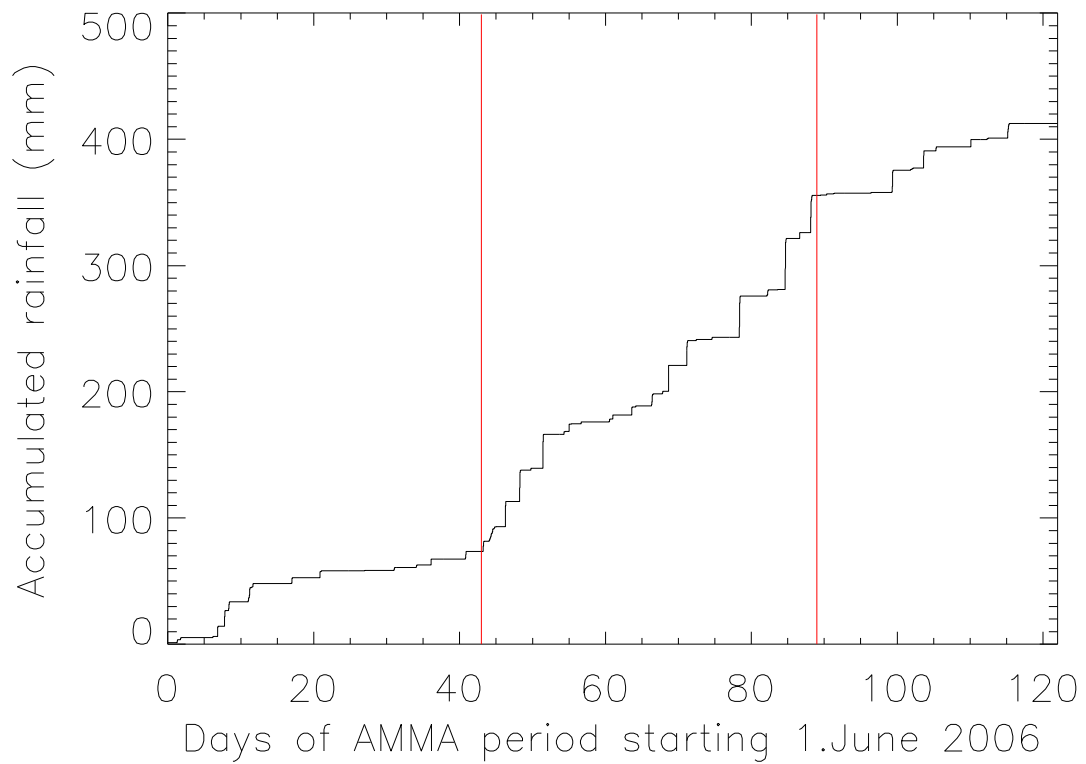
737 **Figures**

738



739

740 **Figure 1:** An example of an observed daily time series as obtained by the surface station at
741 Niamey airport. This time series is for 11th August 2006, when a cold pool crossing was
742 identified at 03:15 Local Time (denoted by vertical red line). Black lines denote the borders of
743 the time-windows used for the analysis. Solid lines correspond to left-hand axis and dashed
744 lines to right-hand axes. Data recorded every second and averaged at minute intervals.

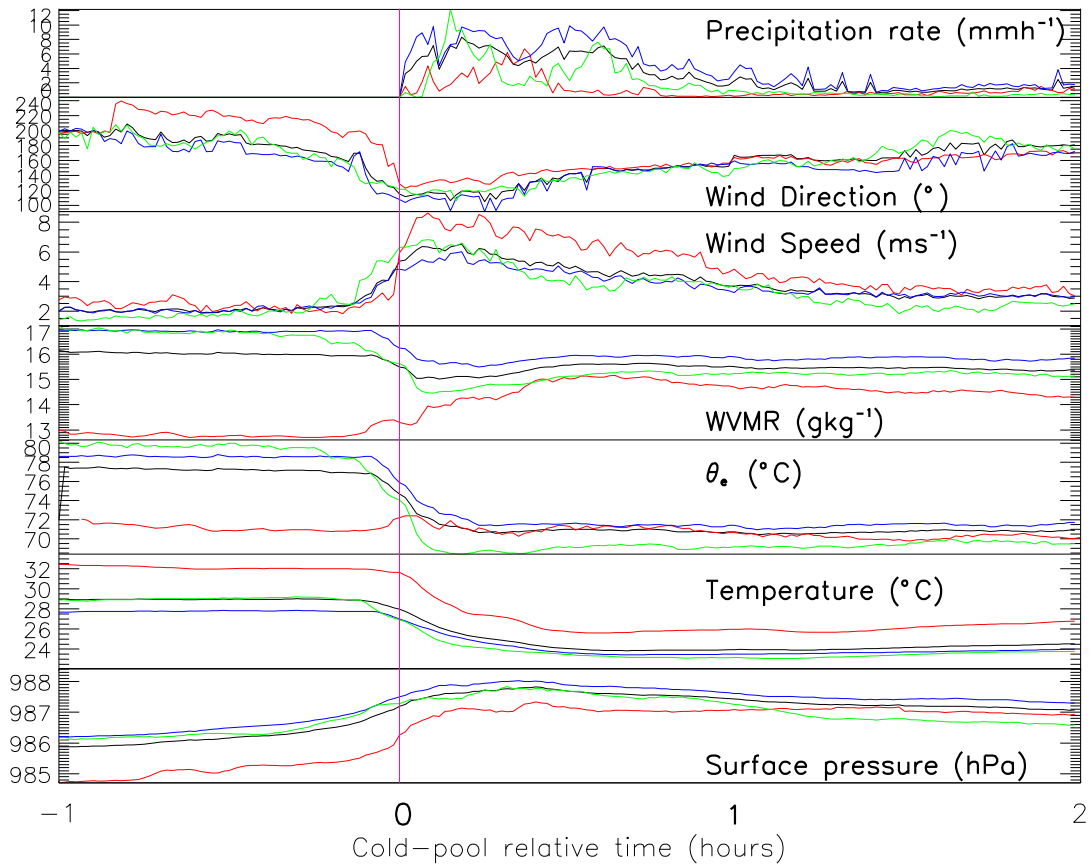


745

746 **Figure 2:** Total accumulated rainfall from Niamey ARM surface station data. Red lines
 747 separate three seasonal periods used in this study: "Pre-monsoon" (1st June 2006 – 12th July
 748 2006); "Monsoon" (13th July 2006 – 27th August 2006); "Retreat" (27th August 2006 – 30st
 749 September 2006).

750

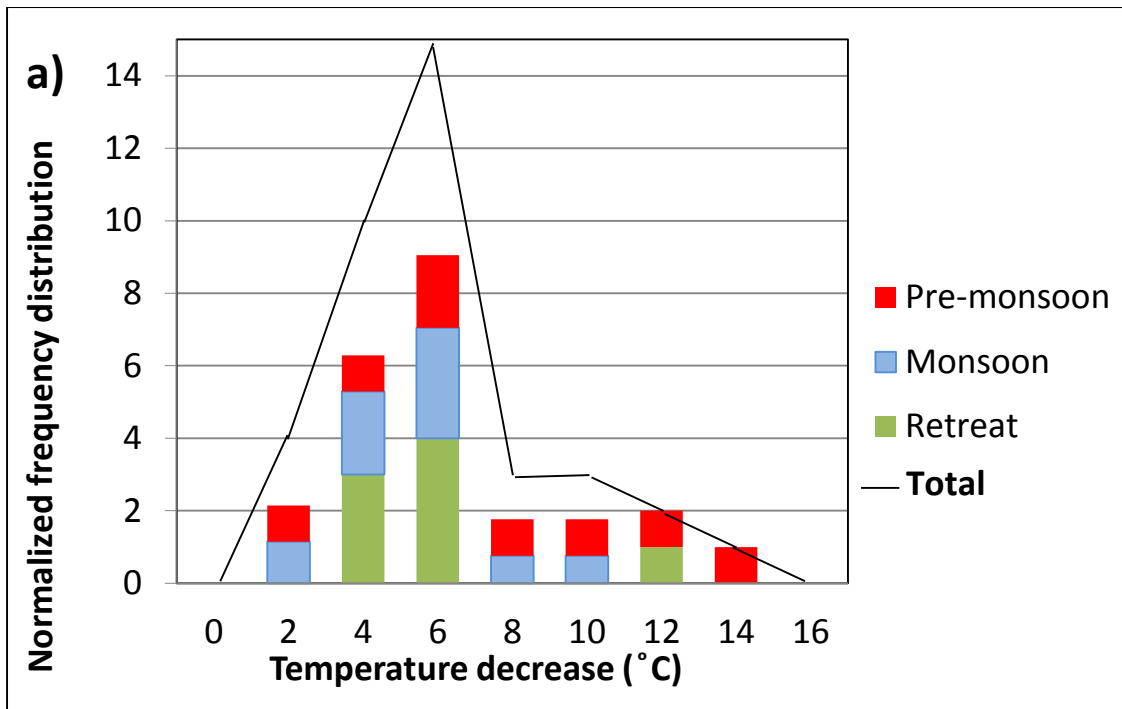
751



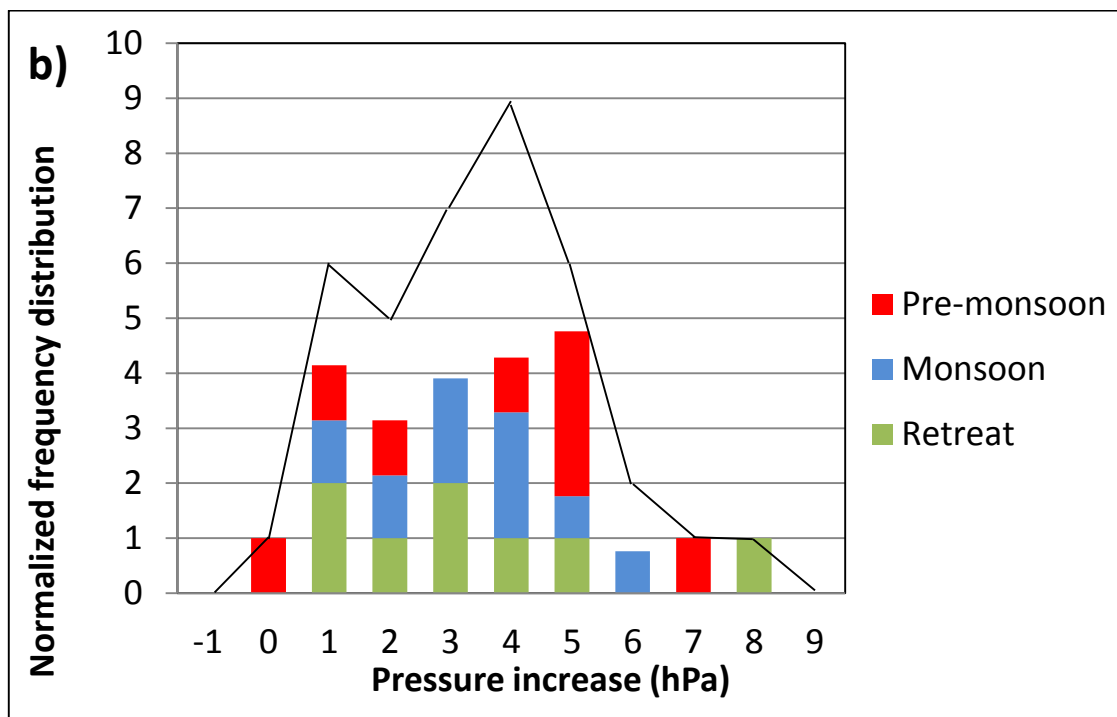
752

753 **Figure 3:** Composite cold pools obtained from averaging variables of all cold pools around
 754 the crossing time. Black line is for the whole period, red for the Pre-Monsoon period, blue for
 755 the Monsoon and green for Retreat. The vertical pink line shows the cold pool crossing time.

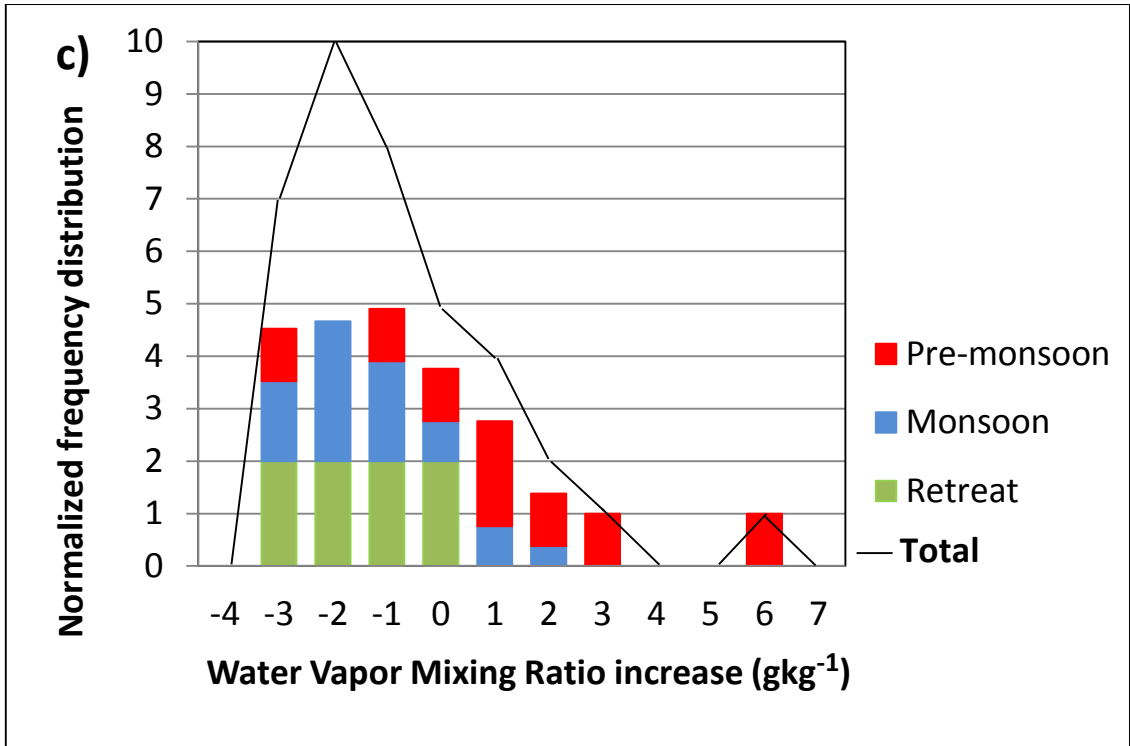
756



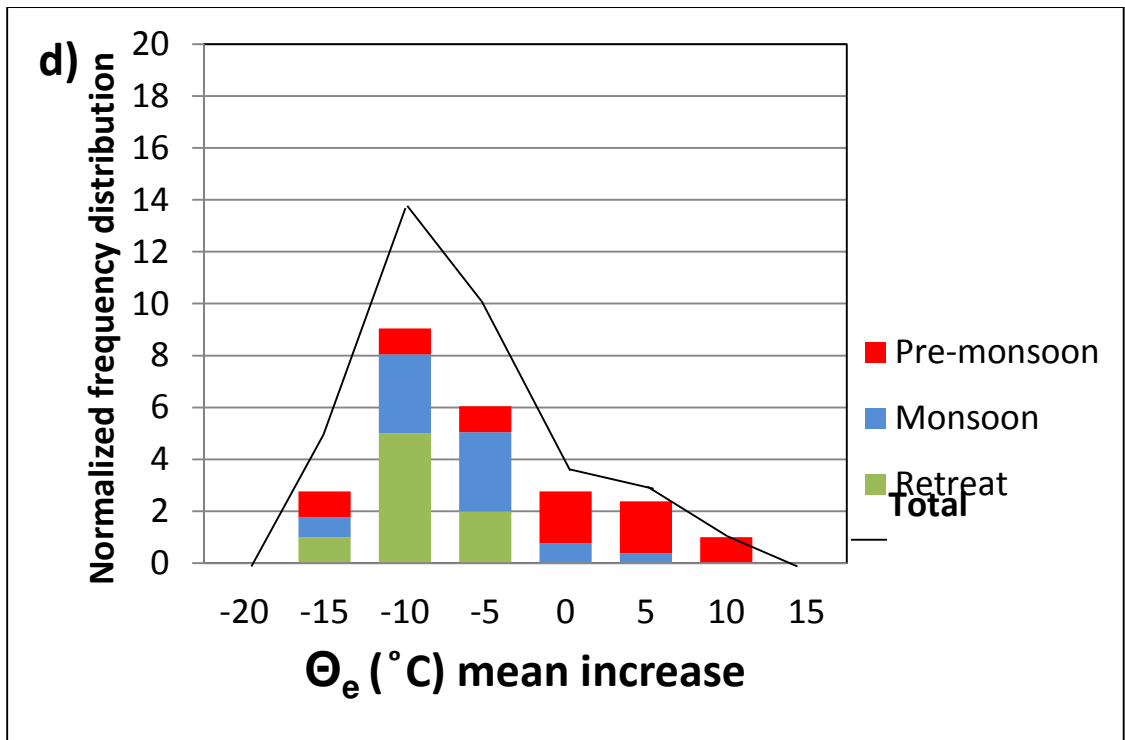
757



758



759



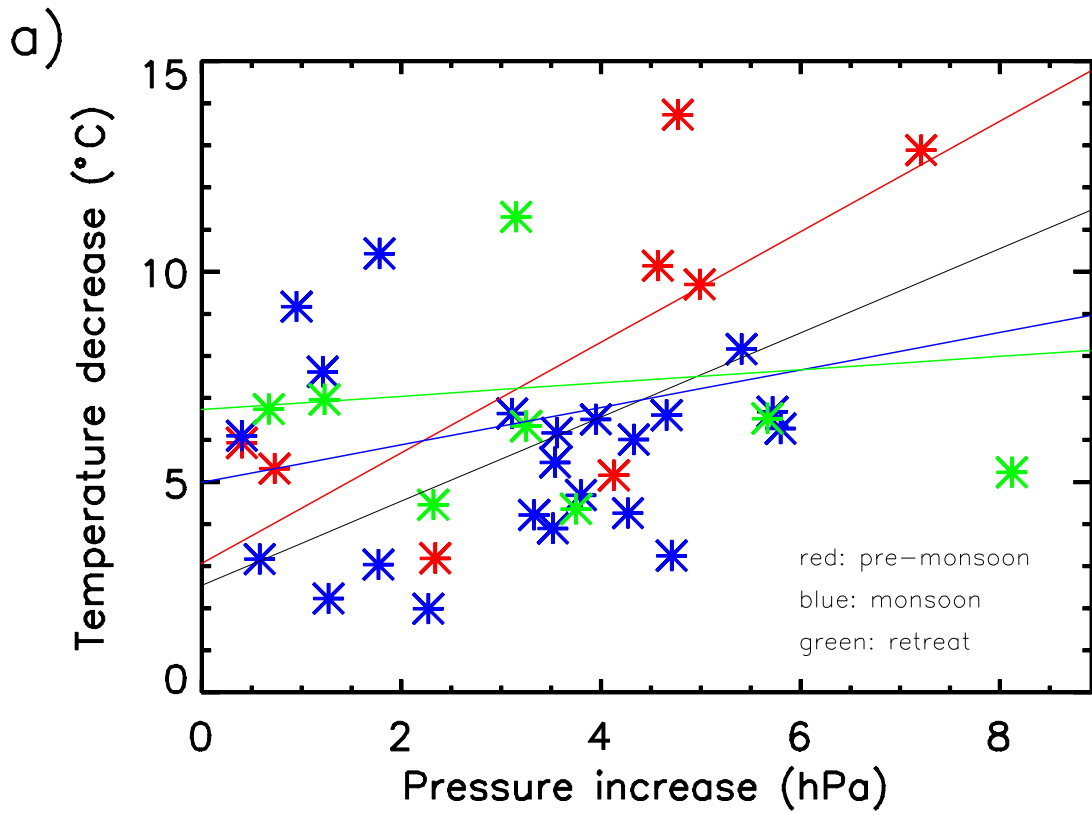
760

761 **Figure 4:** Changes in specified thermodynamic variables from cold pools: a) Decrease in
 762 temperature; b) Increase in pressure; c) Increase in WVMR; d) Increase in mean Θ_e .

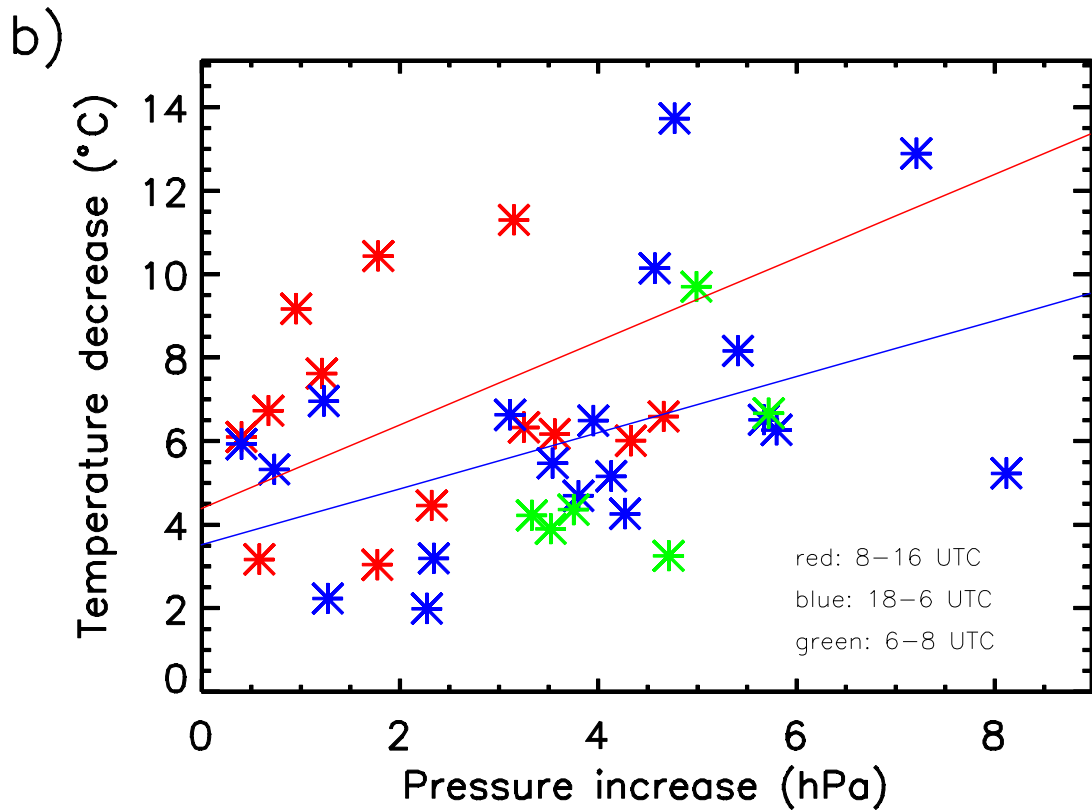
763 Colouring represents the sub-periods (red: Pre-monsoon, blue: Monsoon, green: Retreat).

764 Number of events in each season is normalised to allow a comparison between seasons (see

765 text) with the black line showing total (unnormalised) distributions.

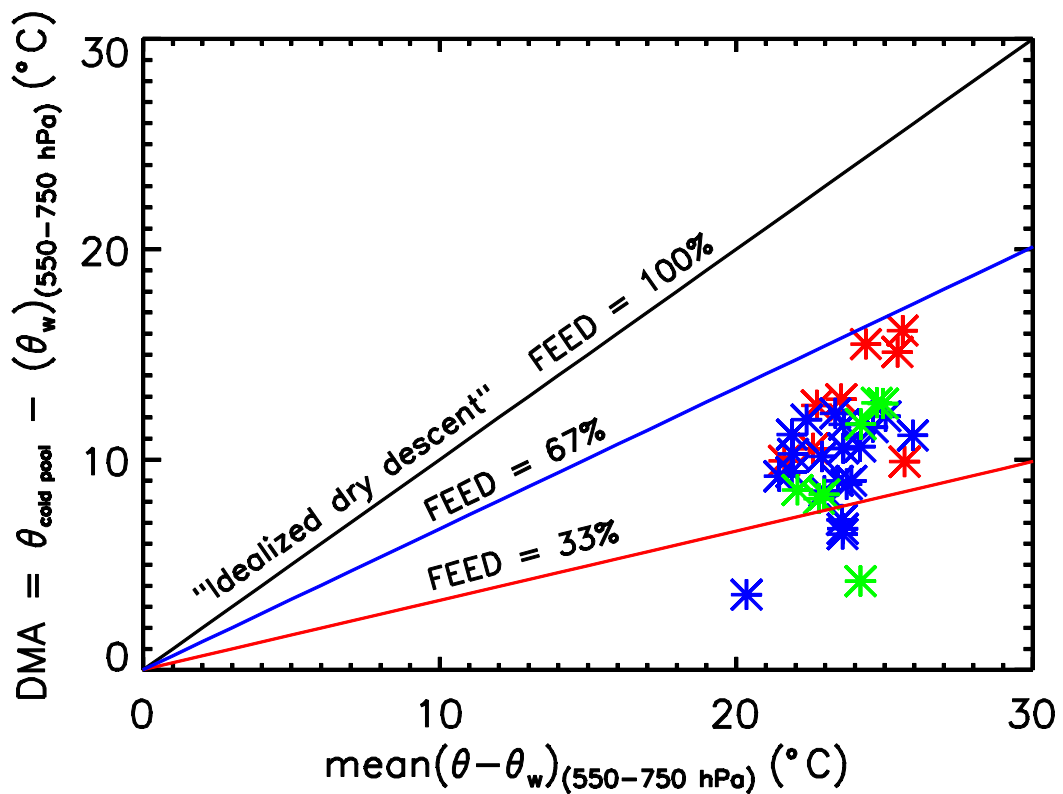


766

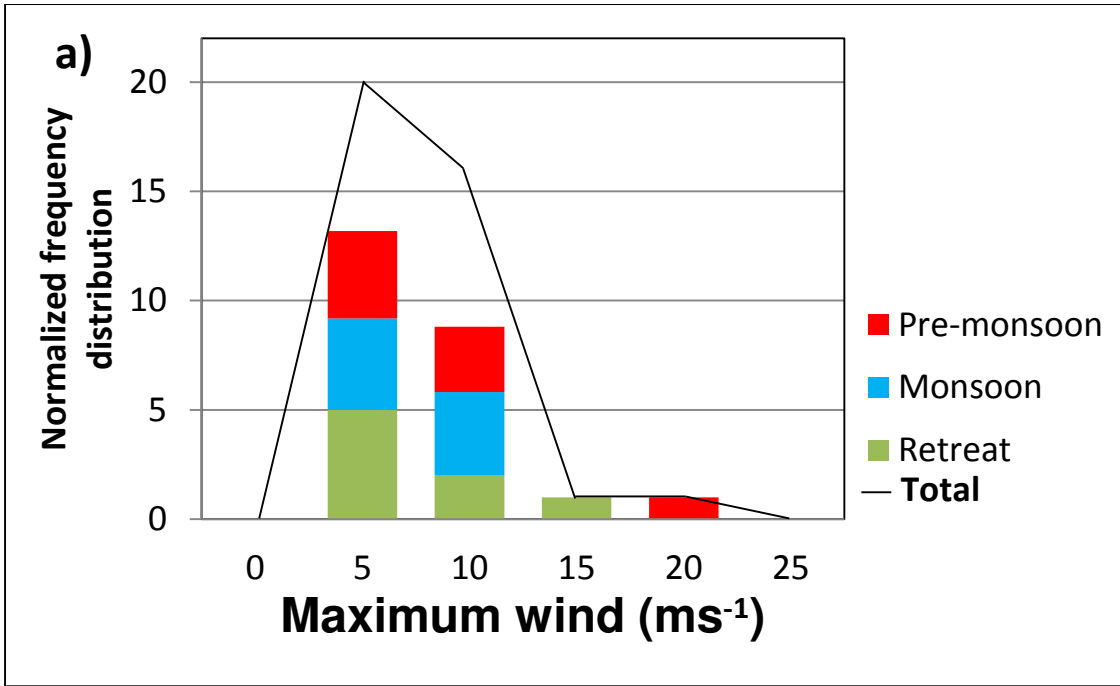


767

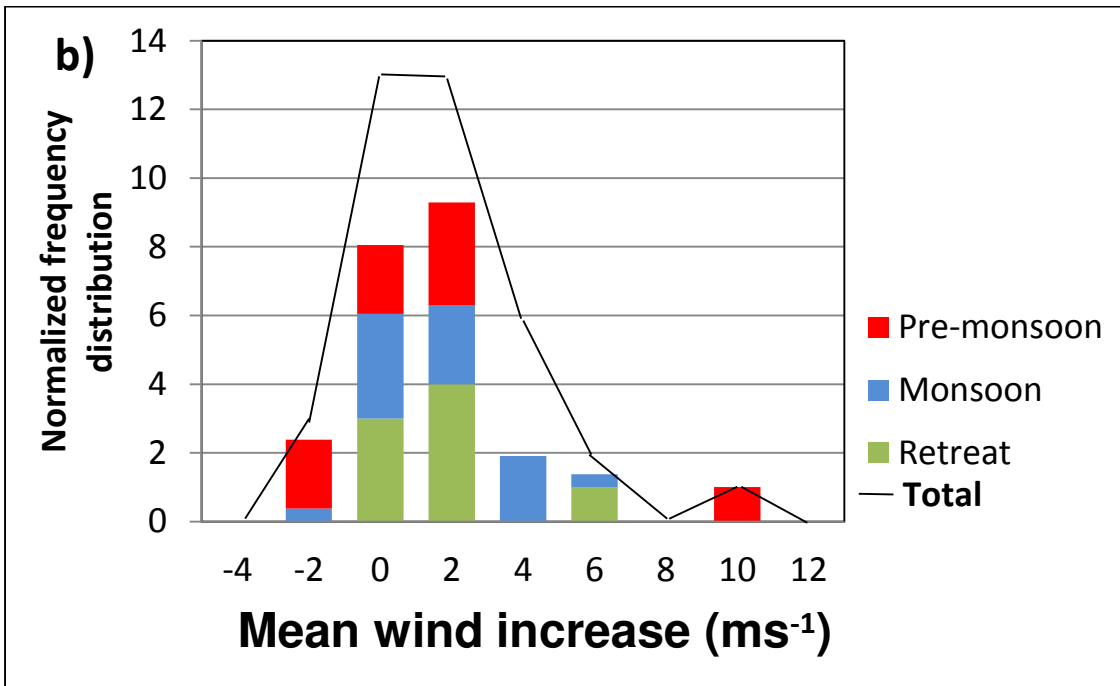
768 **Figure 5** Pressure increases and temperature decreases from cold pools. Colouring in (a)
 769 represents the whole period and sub-periods as in Figure 3. Colouring in (b) represents the
 770 time of day (red: 8 – 16 UTC, blue: 18 – 6 UTC, green: 6-8 UTC, there were no events between
 771 16 and 18 UTC).
 772



773
 774
 775 **Figure 6:** Departure from Moist Adabat ($DMA = \theta_{cold pool} - mean(\theta_w(550 \text{ to } 750 \text{ hPa}))$) versus
 776 mid-level dryness defined using the difference between mean ($\theta(550 \text{ to } 750 \text{ hPa})$) and mean (θ_w
 777 ($550 \text{ to } 750 \text{ hPa})$). Colouring of points represents the sub-periods as in Figure 3. Diagonal lines
 778 represent constant Fractional Evaporational Energy Deficit (FEED) of 100% (black), 67%
 779 (blue) and 33% (red).



780



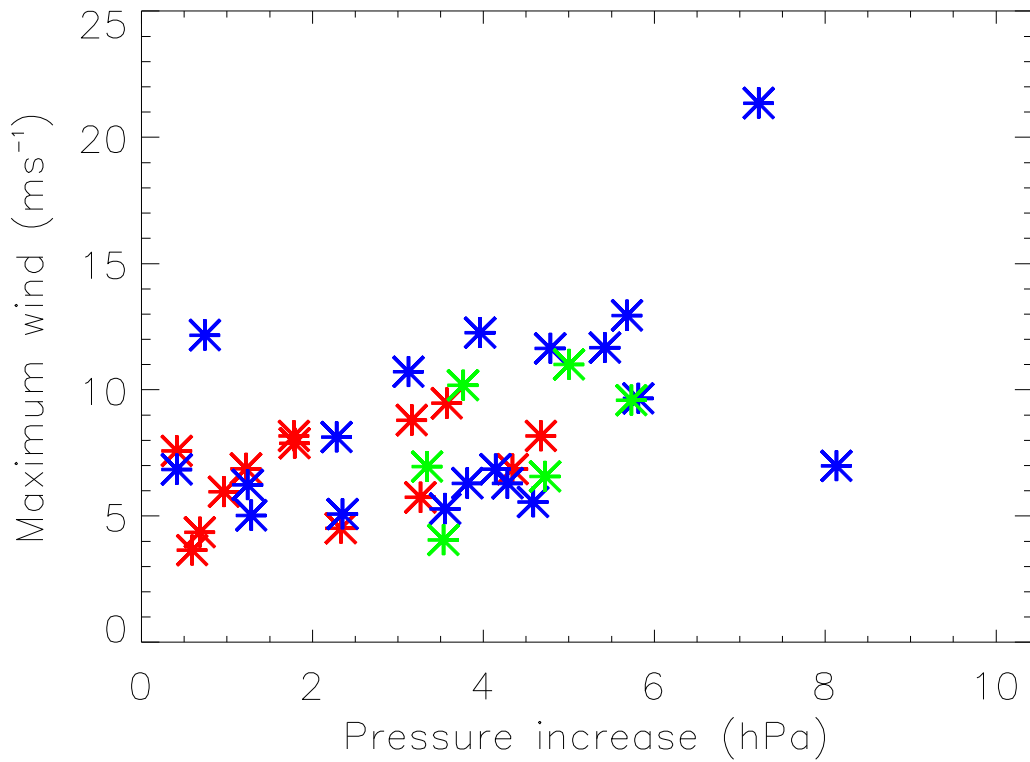
781

782

783 **Figure 7:** As Figure 4, but for (a) 10m wind gusts and (b) mean wind increases.

784

785



786

787 **Figure 8:** Cold pool pressure increases and maximum wind gusts. Colours represent different
 788 times of day (red: 8-17 UTC, blue: 19-6 UTC, green: 6-8 UTC, no cold pool crossed between
 789 17-19 UTC).

Non-Rendered Figure 1

[Click here to download Non-Rendered Figure: Figure1.png](#)

Non-Rendered Figure 2

[Click here to download Non-Rendered Figure: Figure2.png](#)

Non-Rendered Figure 3

[Click here to download Non-Rendered Figure: Figure3.png](#)

Non-Rendered Figure 4a

[Click here to download Non-Rendered Figure: Figure4a.png](#)

Non-Rendered Figure 4b

[Click here to download Non-Rendered Figure: Figure4b.png](#)

Non-Rendered Figure 4c

[Click here to download Non-Rendered Figure: Figure4c.png](#)

Non-Rendered Figure 4d

[Click here to download Non-Rendered Figure: Figure4d.png](#)

Non-Rendered Figure 5a

[Click here to download Non-Rendered Figure: Figure5a.png](#)

Non-Rendered Figure 5b

[Click here to download Non-Rendered Figure: Figure5b.png](#)

Non-Rendered Figure 6

[Click here to download Non-Rendered Figure: Figure6.png](#)

Non-Rendered Figure 7a

[Click here to download Non-Rendered Figure: Figure7a.png](#)

Non-Rendered Figure 7b

[Click here to download Non-Rendered Figure: Figure7b.png](#)

Non-Rendered Figure 8

[Click here to download Non-Rendered Figure: Figure8.png](#)